PCCP

Accepted Manuscript

This is an *Accepted Manuscript*, which has been through the Royal Society of Chemistry peer review process and has been accepted for publication.

Accepted Manuscripts are published online shortly after acceptance, before technical editing, formatting and proof reading. Using this free service, authors can make their results available to the community, in citable form, before we publish the edited article. We will replace this *Accepted Manuscript* with the edited and formatted *Advance Article* as soon as it is available.

You can find more information about *Accepted Manuscripts* in the **Information for Authors**.

Facile synthesis and enhanced microwave absorption property of novel hierarchical heterostructures based on Ni microsphere/CuO nano-rice core-shell composite

Biao Zhao [a], Gang Shao [a, *], Bingbing Fan [a], Wanyu Zhao [a], Rui Zhang [a, b, *]

ABSTRACT: A novel hierarchical heterostructure of Ni microspheres/CuO nano-rices was fabricated using a simple two-step process. The CuO rices were densely deposited on the surfaces of Ni microspheres. The phase purity, morphology, and structure of composite heterostructures are characterized by X-ray diffraction (XRD), field emission scanning electron microscopy (FESEM), energy dispersive 10 X-ray spectroscopy (EDS), and transmission electron microscopy (TEM). Different structured Ni/CuO composite heterostructures are also investigated by adjusting the volume ratio of the reactants. The core-shell rice-like CuO-coated Ni exhibits better antioxidation capability than pure Ni due to the presence of the barrier effect of the CuO shell, which is revealed by the thermalgravimetric analysis (TGA). In comparison with pristine Ni microspheres and CuO nanoflakes, the Ni/CuO composites exhibit excellent microwave absorption properties. Moreover, the amounts of CuO plays a vital role on the microwave attenuation of Ni/CuO composites. The 15 Ni/CuO heterostructures prepared at 0.017 M Cu^{2+} exhibit the best electromagnetic wave absorption capabilities. A minimum reflection loss reaches –62.2 dB (>99.9999% microwave absorption) at 13.8 GHz with the only thickness of 1.7 mm. The effective absorption (below -10 dB) bandwidth can be tuned between 6.4 GHz and 18.0 GHz by tuning absorber thickness of 1.3-3.0 mm. Thus, the Ni/CuO composites possess a fascinating microwave absorption performance as a novel absorbing material with strong absorption, wide-band and thin thickness.

20 1. Introduction

Nowadays, the explosive usage of electromagnetic wave devices, such as wireless networks, communication equipment, and personal digital devices, results in serious electromagnetic interference (EMI) problems in both military and civil 25 applications.[1-5] EMI not only impedes the functionality of electronic devices but also harms humans. Thus, in order to deal with this issue, considerable attention has been paid to the design and development of highly efficient EM wave absorbing materials,[6-8] which can absorb microwaves effectively and 30 convert EM energy into thermal energy or dissipate microwaves.[9-11] Microwave absorbing materials are now required to have the advantages of lightweight, thin thickness, wide absorption bandwidth, strong absorption and simple operation.[12-14]

35 The traditional absorbers, such as ferrite,[15-17] have strong absorption properties, but the thickness required is too large. Therefore, some kinds of composites, especially core-shell structured composites, such as Fe/B_2O_3,[18] Fe-Silica nanoparticles,[19] Fe_3O_4-Poly(3,4-ethylenedioxythiophene),[20] 40 Fe_3O_4 microspheres/polyaniline,[21] Fe_3O_4/carbon Nanorods,[22]

Fe_3O_4/ZnO nanorods,[23] and Fe_3O_4/SnO_2 nanorods [24] show the better microwave absorption performance than the pure core or shell materials. Therefore, synthesis of dielectric–magnetic composite with well-defined structures is beneficial for excellent 45 microwave absorption capabilities.

Nickel as a magnetic microwave absorbent has attracted great interest from many researchers, because of high permeability at GHz frequency ranges, high saturation magnetization, easy preparation, as well as low cost.[25-29] However, the high 50 conductivity results in the rapid decrease in high frequency permeability due to eddy current losses induced by the electromagnetic wave.[30] Therefore, for purpose of optimizing microwave absorption ability, an efficient strategy is to cover the magnetic Ni particles by an inorganic and nonmagnetic coating to 55 create a core/shell microstructure.

As an important p-type semiconductor, CuO, with narrow band gap (E_g = 1.2 eV), has attracted great attention due to its unique properties and widespread potential applications in optical switches, anode materials, field emitters, catalyst, gas sensors, 60 photoelectrode and high-temperature microconductors.[31-36]

Recently, CuO has been revisited as an efficient material for the preparation of microwave absorbing materials.[37-40] For example, copper oxide-carbon fiber composites have been synthesized by annealing copper/carbon fibers in air and the minimum reflection 5 loss is −29.6 dB at 7.8 GHz. [37] Zeng and co-workers have reported that the strongest reflection loss of CuO/Co/carbon fiber is −42.7 dB at 10.8 GHz. [38] The CuO/Cu$_2$O-coated Ni nanocapsules have also reported by the arc discharge method and the optimal reflection loss value of −47.8 dB was observed at 10 14.4 GHz. [40] From above results, it can conclude that CuO composites show excellent microwave capabilities.

To the best of our knowledge, the studies on the preparation of CuO rice-coated Ni core/shell composite have never been reported. Herein, we report a facile method to synthesize the 15 core-shell structured composites with Ni cores and rice-like CuO shells. The microwave absorption performances of Ni, CuO and Ni/CuO composites were investigated in the frequency of 2-18 GHz. Compared with pure Ni and CuO, rice-like CuO-coated Ni composites show the best microwave absorption properties. 20 Moreover, the effect of CuO contents on structures and microwave absorption properties of Ni/CuO composites were also investigated in detail.

2.   Experimental section

2.1. Materials. All chemicals were of analytical grade and used 25 without further purification. Trisodium citrate, anhydrous ethanol, and N$_2$H$_4$·H$_2$O (80%) were purchased from Guangfu Chemical Co. Ltd. (Tianjin, China). Nickel chloride hexahydrate (NiCl$_2$·6H$_2$O), 1,2-isopropanol, ammonia (NH$_3$·H$_2$O), copper chloride hexahydrate (CuCl$_2$·2H$_2$O) and sodium acetate were 30 purchased from Xilong Chemical Reagent Co. Ltd. (Guangdong, China). The experimental procedure is schematically shown in Fig.1.

2.2. Synthesis of monodispersed Ni microsphere. The Ni microspheres were prepared by a solvothermal method, which 35 was described in our pervious literature.[41] Briefly, NiCl$_2$·6H$_2$O (1.2 g), sodium acetate (3.0 g) and trisodium citrate (0.3 g) were first dissolved in 1,2-isopropanol (60 mL). Then N$_2$H$_4$·H$_2$O (6.0

mL) was introduced into above solution. After that, the mixture was transferred into a Teflon-lined stainless-steel autoclave. The 40 autoclave was maintained at 140 °C maintained for 15 h and then allowed to cool to room temperature. Finally, the black precipitates were washed with water and ethanol and dried at 60 °C for 12 h in a vacuum.
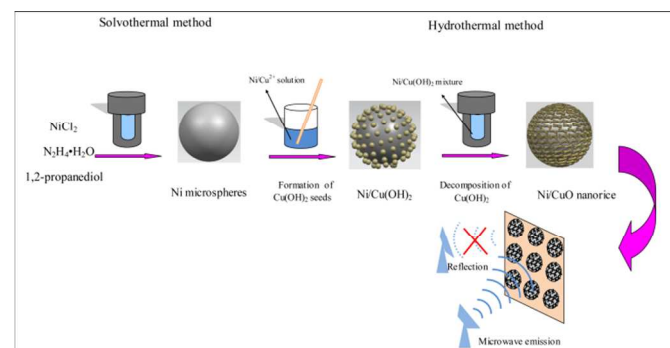

45 **Figure   1.**   Schematic   illustration   of   rice-like   Ni/CuO heterostructures formation route and their application

2.3. Synthesis of CuO nanoflakes. CuCl$_2$·2H$_2$O (0.36 g) was dissolved in a mixture of distilled water (60 mL) and ammonia (2 mL) under continuously stirring (30 min). The final mixture was 50 transferred   into   a   Teflon-lined   autoclave   and   heated hydrothermally at 150 °C for 15 h. The products were harvested via washing six times with ethanol and water.

Table 1. Experimental parameters (material, temperature, time, and so on) for the preparation of three Ni/CuO Composites

Sample no.	Raw reagents	Hydrothermal temperature and time	Morphology of products
S-1	0.05 g Ni + 0.18 g CuCl$_2$·2H$_2$O + 2mL NH$_3$·H$_2$O + 60mL H$_2$O	150 °C 15 h	CuO rice - coated Ni composite
S-2	0.05 g Ni + 0.36 g CuCl$_2$·2H$_2$O + 2mL NH$_3$·H$_2$O + 60mL H$_2$O	150 °C 15 h	CuO rice-coated Ni composite
S-3	0.05 g Ni + 0.54 g CuCl$_2$·2H$_2$O + 2mL NH$_3$·H$_2$O + 60mL H$_2$O	150 °C 15 h	Ni@CuO nanoflke composite

55 **2.4. Synthesis of CuO rice-coated Ni core/shell composites.**

The as-prepared Ni microspheres (0.05 g) and $CuCl_2\cdot2H_2O$ (0.36 g) were first dispersed in distilled water (60 mL). Secondly, the ammonia (2 mL) was added into the solution. Then the obtained solution was transferred into a Teflon-lined autoclave. The Teflon-lined autoclave was sealed and heated at 150°C for 15 h and cooled to room temperature. Lastly, the final product was separated by centrifugation, washed alternately for several times with distilled water and ethanol, and dried at 60 °C under vacuum. Two other types of Ni/CuO samples are prepared for comparison with a similar method. The preparation process of three Ni/CuO composites is summarized in Table 1.

2.5. Characterization. The morphology of the synthesized products was examined by field emission scanning electron microscope (FESEM, JSM-7001F) and transmission electron microscope (TEM, JTM-2100). The crystallographic phases of the as-prepared samples were determined by powder X-ray diffraction method (XRD, XD-3, Beijing Purkinje General Instrument Co. Ltd. Cu Kα radiation source, λ=0.15406 nm). The elemental composition of products was examined by energy disperse X-ray spectrometry (EDS, Oxford Instruments) associated with FESEM. The thermogravimetric analyzer (TGA) was studied by a STA 409/PC simultaneous thermal analyzer (Netzsch, Germany) from 50 ℃ to 800 ℃ with a heating rate of 10 °C/min in flowing air. These products were uniformly blended with paraffin matrix with a mass ratio of 7:3 (70 wt %), and the microwave absorbing devices were prepared with a cylinder shape (outer diameter of 7 mm and inner diameter of 3.04 mm) for microwave measurements. The complex permittivity ($\varepsilon_r = \varepsilon' - j\varepsilon''$) and permeability ($\mu_r = \mu' - j\mu''$) of the composites were measured in the 2.0-18.0 GHz on a vector network analyzer (Agilent N5244A).

3. Results and discussion

3.1. Characterization of Ni@CuO heterostructures.

The crystal structures associated with Ni microspheres, CuO nanoflakes, and Ni/CuO heterostructures have been examined by XRD, as illustrated in Fig.2. Compared with Ni (JCPDS card No. 04-0850) and CuO (JCPDS card No. 05-0661), Fig.2a,b shows all the diffraction peaks can be assigned to face-centered cubic Ni and monoclinic phase structure of CuO. Fig.2c shows two mixed phases of face-centered cubic Ni and monoclinic CuO. The circle indicates the peaks stemming from monoclinic CuO (JCPDS card No. 05-0661), while the others come from face-centered cubic Ni (JCPDS card No. 04-0850). No other impurity diffraction peaks are discovered, which confirm the purity of the products. The surface analysis of the as-prepared Ni/CuO composites were further investigated by XPS as shown in Fig. S1. The peaks located at 933.4 eV and 953.3 eV were assigned to Cu $2p_{3/2}$ and Cu $2p_{1/2}$, respectively. In addition, the strong shake-up peaks confirmed the Cu(II) oxidation state and excluded the possible existence of the Cu_2O phase. [42]
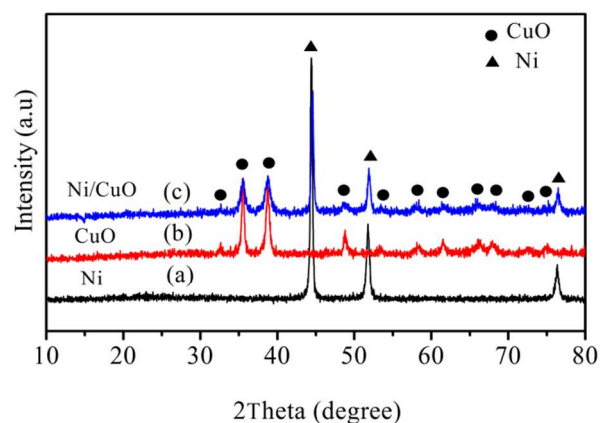

Figure 2. XRD pattern of (a) Ni microspheres, (b) CuO nanoflakes, and (c) Ni@CuO heterostructures, respectively.

Fig.3 exhibits FESEM micrographs of Ni@CuO composites with different magnification after hydrothermal treatment at 150 °C for 15 h. It can be observed from Fig.3a,b that the products are composed of CuO rices-coated smooth Ni microspheres heterstructures with the diameter of 1.0-1.2 μm. The high-magnification SEM image (Fig.3c) shows that rice-like CuO/Ni composites hold rough surfaces, which result from compactly aggregated panicle-shape CuO nanostructures. Moreover, an individual rice-like CuO/Ni composites with a rough surface is shown in Fig.3d. This hierarchical rice-like CuO/Ni may pave a way to microwave absorption due to these rough surfaces.
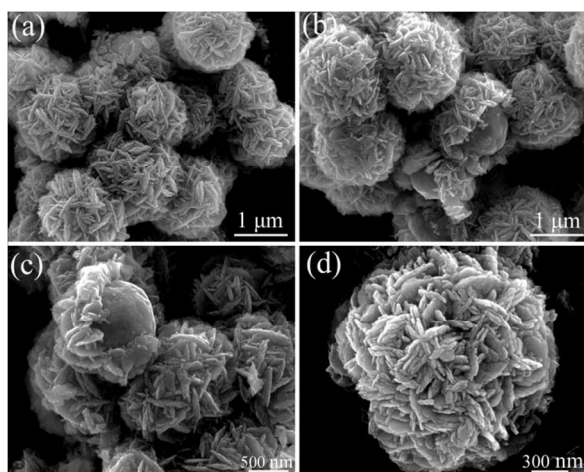
Figure 3. FESEM images of the Ni microsphere-CuO rice core-shell structures (a,b) panoramic and (c,d) magnified.

For comparison, the shapes of the prepared Ni and CuO products were also investigated as shown in Fig.4(a,b). As shown in Fig.4a, the surface of pristine Ni microspheres is relatively smooth with about 1.0 μm in diameter. Fig.4b shows the morphology of CuO products. The CuO samples possess approximately uniform flake-like morphology with the diameter and thickness of 0.6−1.0 μm and 20 nm, respectively. The nanoflakes are gathered up to form coral-like hierarchical structures with the diameter of about 3.0 μm. Fig.4(c,d) exhibit the EDS patterns of Ni microspheres (Fig.4c) and CuO nanoflakes (Fig.4d). It can be observed that the Ni sample consists of only element Ni, however, CuO nanoflakes are comprised of element Cu and element O, which indicate no detectable contamination in both pure Ni system and CuO system.
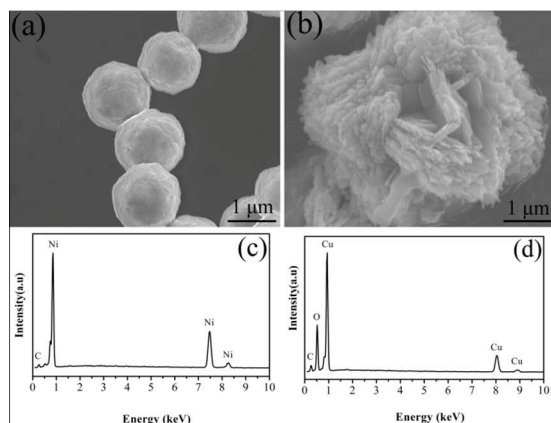

Figure 4. FESEM images of (a) the Ni microspheres and (b) the

CuO nanflakes; EDS patterns of (c) Ni microspheres and (d) CuO nanoflakes.

The FESEM image of an individual Ni/CuO core−shell composite is shown in Fig.5a. The smooth Ni microspheres were tensely covered by rice-like CuO. The EDS profile of the Ni/CuO, shown in Figure 5b, indicates that the obtained heterostructures are composed of Ni, Cu and O elements. The C element is attributed to the rubberized fabric, which is used for pasting the samples. Pt peaks are also observed in the spectrum because the SEM sample was prepared by sputtering of platinum onto the sample. The elemental mappings of Ni/CuO were performed in Fig.5c-e. One can see that the Ni element can be detected in the core region, while the O element and Cu element exhibit larger areas compared with Ni. This confirms the core-shell structures with Ni cores and CuO shells have been formed after hydrothermal process.
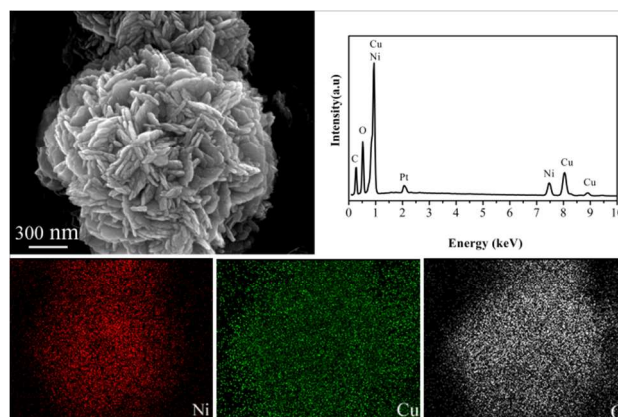

Figure 5. (a) FESEM image of an individual Ni/CuO core−shell heterostructure, (b) EDS pattern of Ni/CuO composite and (c-e) elemental mappings of Ni, Cu and O.

In order to get more information about microstructure of Ni/CuO composite, TEM and HR-TEM images of Ni/CuO composites were performed in Fig.6. The core-shell structure of Ni/CuO composite can be clearly observed from Fig.6. The inset SAED pattern of the CuO particles indicated that CuO particles are polycrystalline (Fig.6a). The HRTEM image (inset of Fig.6b) displays that the lattice spacing was 0.276 nm, which is in good agreement with the (110) lattice spacing of CuO. Based on the SEM and TEM results, it can be concluded that the CuO was deposited on the surface of Ni, the core-shell composites were obtained under this procedure.
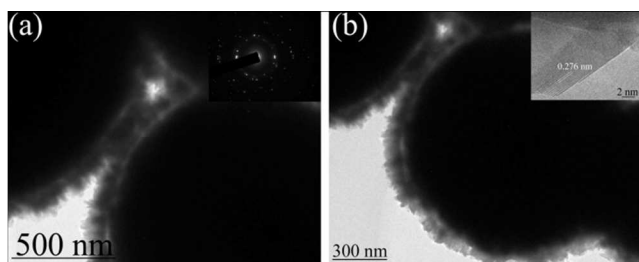
Figure. 6 Typical TEM and HRTEM images of the as-prepared Ni/CuO structures: (a) low magnification, inset of (a) shows the SAED pattern; (b) high magnification; inset of (b) shows the

5 HRTEM.

Fig.7 shows the morphologies of the products with different molar ratio of the $CuCl_2 \cdot 2H_2O$ to Ni microspheres in the precursor solution. It is worth noting that the surfaces of all samples turns coarser compared with the pristine Ni

10 microspheres, which can be ascribed to the successful coating of the CuO nanoparticles on the primary Ni surfaces. Moreover, control of shape and coverage density of CuO materials was achieved by adjusting the concentration of precursor (Cu^{2+}). When the molar ratio of the $CuCl_2 \cdot 2H_2O$ to Ni microspheres in

15 the precursor solution is 1: 0.85 (S-1), it can be found (Fig.7a,b) that plenty of CuO rices are formed on the surface of the Ni microspheres. However, the thickness of CuO shell is thin because of low concentration of precursor (Cu^{2+}). When the molar ratio is increased to 2: 0.85 (S-2), it can be observed that

20 the aggregation phenomenon occurred and CuO rices are densely deposited on the smooth surfaces of Ni microspheres to form coarser thick CuO shells (Fig.7c,d). When the molar ratio is increased continuously to 3:0.85 (S-3), a layer of dense CuO nanflakes grown on Ni microspheres is generated (Fig.7e,f).

25 From above analysis, the structures and coverage density of CuO shells can be effectively tuned by choosing an appropriate concentration of Cu^{2+}.
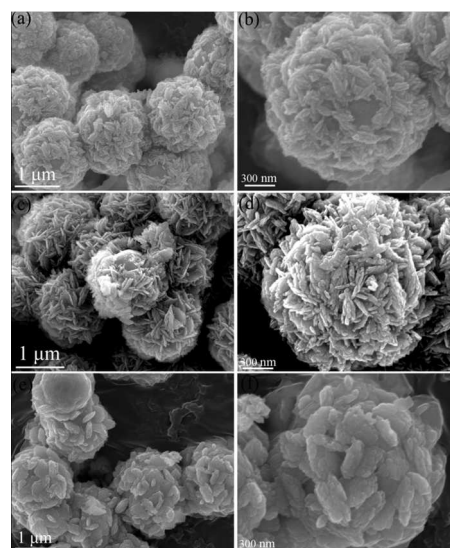

Figure 7. FESEM images of hierarchical Ni/CuO core-shell
30 heterostructures with different molar ratio: (a, b) S-1; (c, d) S-2; (e, f) S-3.

3.2. Electromagnetic properties of Ni/CuO composite

The electromagnetic properties of the Ni, CuO and the Ni/CuO core/shell composites were investigated in the frequency
35 range from 2 to 18 GHz in this study. The frequency dependence complex permittivity and permeability for five materials are shown in Fig.8. The real permittivity (ε') and real permeability (μ') represent the storage ability of electromagnetic energy, while the imaginary permittivity (ε'') and imaginary permeability (μ'')
40 are connected with the energy dissipation and magnetic loss, respectively. [20, 43] The real (ε') and the imaginary (ε'') parts of the relative complex permittivity are shown in Fig.8a,b. It is noted that for Ni the values of the real and imaginary parts of the permittivity are very high, with permittivity decreases as the
45 frequency increases (Fig.8a,b), but the value of the real and imaginary parts of the permeability vary a lot with frequency increases (Fig.8c,d). The complex permeability of Ni was lower than that of complex permittivity, which result in poor impedance match. The impedance match requires that the relation between
50 permittivity and permeability tends to be close, which can achieve zero-reflection at the front surface of the materials. [44] The higher permittivity of the absorber is harmful to the impedance match, [45] thus leads to weak microwave absorption. For Ni/CuO

and CuO, the values of the real part of the permittivity are relatively stable with frequency increases and the S-1 sample shows high ε′ values (Fig.8a), which are due to space charge polarization because of the heterogeneity of the material. The

5 presence of semiconductor CuO coating on the surface of Ni microspheres results in the formation of more interface and space charge accumulating at the interface, which contributes to higher microwave absorption in the composites.[15] From the Fig.8b, one can also observe that there exist frequency intervals in which the

10 permittivity exhibits resonant characteristics. Multi-peaks can also be observed near the resonant frequencies on the ε″ curve. These phenomena are the typical characteristics of nonlinear resonant behaviors. [46] The exact mechanism of these multi-peaks is still underway. For sample S-1, the resonant frequencies of

15 permittivity in current band range are of 3.8, 9.9 and 15.6 GHz, respectively. According to previous publications, [46, 47] dielectric resonances at 3.8 GHz should be related with Ni particles. However, heterojunction capacitance generated at the interface of CuO rices and Ni microspheres could induce the other two

20 resonant peaks (9.9 and 15.6 GHz), which are similar with previous reports by Shi [46] and Liu [47]. Generally, nonlinear dielectric resonance originates from the cooperative consequence of Ni cores, core/shell interfaces and the dielectric CuO shells. The variation in μ′ and μ″ as a function of frequency of the

25 composites are shown in Fig.8c,d. The μ′ values of Ni/CuO and CuO samples obviously decrease with increasing frequency in the 2.0–18.0 GHz range (Fig.8c). For the five samples, the μ″ exhibits broad resonance peaks at 5-7 GHz, which are attributed to natural resonance of Ni. [48] It is worth noting that the μ″ of S-1

30 sample show the highest values among the five samples, which indicates the highest magnetic loss. Based on the complex permittivity and permeability, it can conclude that the S-1 sample may possess improved microwave absorption properties because of good impedance match, high dielectric loss and magnetic loss.
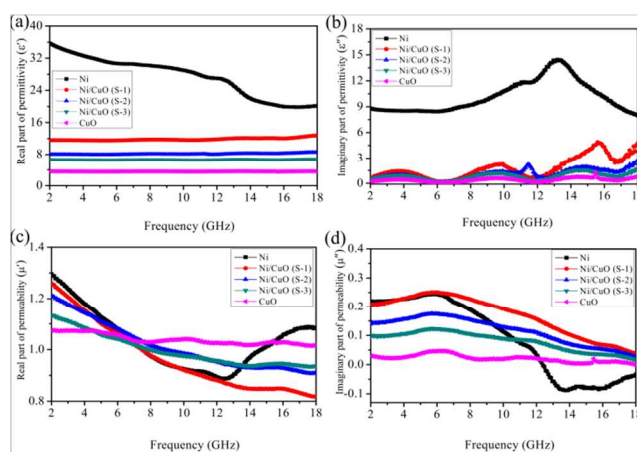

Figure 8. Frequency dependence of the (a) real and (b) imaginary parts of complex permittivity, and the (c) real and (d) imaginary parts of complex permeability for the five as-prepared samples.

40 To compare and evaluate their electromagnetic wave absorption properties, Ni, Ni/CuO core-shell heterostructures, and CuO nanoflakes were uniformly blended in a paraffin matrix (30 wt %), which is transparent to microwave, and assembled into a microwave-absorption device with an outer diameter of 7.00 mm

45 and an inner diameter of 3.04 mm, and the devices were measured in the range of 2−18 GHz. The microwave absorption capabilities of these as-prepared products can be evaluated by the reflection loss (RL) values, which can be calculated based on the complex permeability and permittivity at a given frequency and

50 layer thickness by means of the following equations:[49-51]

$$RL = 20\log\left|(Z_{in} - Z_0)/(Z_{in} + Z_0)\right| \qquad (1)$$

$$Z_{in} = Z_0\sqrt{\frac{\mu_r}{\varepsilon_r}}\tanh\left(j\frac{2\pi f d\sqrt{\mu_r\varepsilon_r}}{c}\right) \qquad (2)$$

where Z_0 is the impedance of free space, Z_{in} is the input characteristic impedance, f is the frequency, c is the velocity of

55 light, and d is the thickness of the composites. The results are shown in Fig.9. As shown in Fig.9a, the three Ni/CuO composites present much stronger microwave-absorption properties than the pristine Ni microspheres and the CuO nanoflakes. For example, when the thickness is 2 mm, the S-1 sample shows the strongest

60 EM-wave absorption with an RL value of −15.6 dB at 11.9 GHz among the five samples. The thickness of the absorber, as one of critical factors, will influence the RL value and the frequency of

maximum absorption. Hence, the reflection loss of Ni/CuO samples with various thicknesses were also simulated. In comparison with S-2 (Fig.9c) and S-3 (Fig.9d), the S-1 (Fig.9b) shows best microwave absorption properties. The lowest reflection loss of the S-1 sample is –62.2 dB at 13.8 GHz with the only thickness of 1.7 mm. The effective absorption bandwidth (below -10 dB) can reach 3.3 GHz (12.4-15.7 GHz) with the absorber thickness of 1.7 mm. In order to confirm the role of core-shell heterostructures on the microwave absorption of Ni/CuO composites, the electromagnetic wave absorption property of the mixture of Ni spheres and CuO nanoflakes have also been investigated and the results are presented in Fig. S2. Compared with the core-shell structured Ni/CuO composite, the mixture of Ni spheres and CuO nanoflakes shows the weak absorption properties. The minimum reflection loss is only –13.6 dB at 10.1 GHz. In current Ni/CuO heterostructure, CuO rices play two roles in our Ni/CuO core-shell structure. One is semiconducting layer, which can improve impedance match by lower the conductivity of Ni particles in low CuO concentration system.[52] The other tone is generation of core-shell structure, which exhibits enhanced resonance at the induced interfaces [53] created by introducing CuO materials onto Ni particles. Therefore, the microwave absorption efficiency was improved dramatically. In this regard, the combination of magnetic materials (Ni) with dielectric materials (CuO) has been proved as good candidate of high efficient microwave-absorption materials. Table 2 shows the microwave absorption properties of typical Ni-based composites and other hybrid composites. [1, 4, 9, 13, 14, 25, 26, 28, 29, 48, 54-56] It can be seen that the rice-like CuO coated Ni microspheres possess stronger EM absorption capability and a thinner absorber thickness and broader absorption bandwidth. It is noteworthy that the peaks shift gradually to lower frequencies with increasing absorber thickness, which can be explained by quarter-wavelength cancellation model that the incident and reflected waves in the absorber are out of phase 180° and leading to the reflected waves in the air-absorber interface are cancelled totally. [57, 58] For quarter-wavelength cancellation, the relationship between d_m and f_m is given by the following equation

$$d_m = \frac{nc}{4f_m\sqrt{|\mu_r \varepsilon_r|}} \quad (n=1, 3, 5\ldots)$$

where μ_r is the complex permeability, ε_r, is the complex permittivity, c is the velocity of light in the free space. The best absorption property of core-shell Ni/CuO composites can be achieved by adjusting the amounts of CuO. The rice-like CuO shell plays a positive role on the attenuation proprieties of the core/shell composites. The CuO shells were deposited on the surface of Ni microspheres to form the special core-shell structure, which introduces metal/dielectric interfaces to induce interfacial polarization. Interfacial polarization always presents in materials comprised of more than one phase composites. [59-62] This kind of polarization arising at the interfaces is due to the migration of charge carriers through different phases of the composite material, which results in charge accumulation at these interfaces. During the activation of electromagnetic wave, a redistribution process of charges occurs periodically between Ni cores and CuO shells, which is beneficial for the microwave absorption. However, for the S-2 and S-3 samples, the amounts of CuO are too high that the cooperation between Ni cores and CuO shells disappears, which leads to poor microwave absorption.
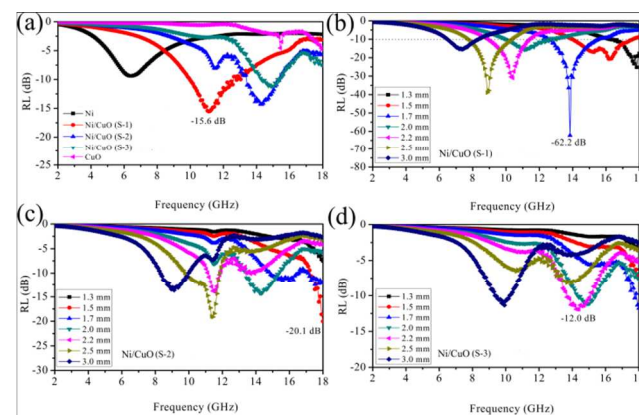

Figure 9. (a) Comparison of reflection losses of the five as-obtained samples with a thickness of 2.0 mm. The reflection losses of (b) S-1, (c) S-2, (d) S-3 samples with various thicknesses.

Table 2 Microwave absorption properties of some reported Ni-based composites and other hybrid composites

Sample	Minimum RL value (dB)	Matching thickness (mm)	Matching frequency (GHz)	Frequency range (RL<-10 dB) (GHz)	Ref.
Octahedral Ni	–40.44	2.5	8.8	7.1–11.2	[25]

Ni fiber	−39.5	3.0	4.8	6.6–8.8	[26]
Urchin-like Ni	−43	2.0	10	8.7–11.5	[28]
Ni chains	−25.29	2.0	9.6	8.3–10.4	[29]
Hexagonal Ni/graphene	−17.8	5.0	3.5	2.7–3.9 11.9–13.5	[48]
FeCo/C/BaTiO$_3$	−41.7	2.0	11.3	9.4–14.5	[1]
nano-flower CoO	−37	2.0	10.5	8–14	[4]
Fe$_3$O$_4$/graphene	−26.4	4.0	5.3	4.5–6.5	[9]
Porous Fe$_3$O$_4$@ZnO-grapheme	−40	5.0	11	10.2–12.1	[13]
Fe$_3$O$_4$/basalt fibers	−31.1	5.0	5.9	5.3–6.5	[14]
γ-Fe$_2$O$_3$–MWNTs/PBO	−32.7	3.7	12.9	11.3–13.8	[54]
Grapheme-polyaniline	−36.9	3.5	10.3	8.2–13.5	[55]
MWCNT-Fe$_3$O$_4$@ZnO	−40.9	3.5	9.8	8.0-12.0	[56]
Rice-like CuO-coated Ni	−62.2	1.7	13.8	12.4-15.7	present work

The dielectric loss factor (tan δ$_ε$ = ε″/ε′) and the magnetic loss factor (tan δ$_μ$ = μ″/μ′) may well explain why the S-1 sample exhibits the best microwave absorption properties, as shown in Fig.10. S-1 sample presents the highest dielectric loss and magnetic loss among the three samples, which indicates the excellent capability of microwave absorption. On the other hand, the S-1 show strong magnetic loss at the low-frequency range and significant dielectric loss at high-frequency range. Such complementarities between the dielectric loss and the magnetic loss imply that the S-1 sample holds excellent EM absorption properties. It is evident that the improved microwave absorption properties for the Ni/CuO composites are a consequence of better electromagnetic matching due to the existence of dielectric CuO shells, as well as its particular 'core/shell' microstructure. Moreover, the unique rice-like CuO structure in S-1 sample is also favourable in the enhancement of EM wave absorption. Rice-like shape can act as isotropic quasi-antennas, favoring the penetration of electromagnetic waves into the composites, which can generate continuous micronetworks and a large-scale vibrating microcurrent.[63, 64] The electromagnetic energy is induced into a dissipative current and consumed in discontinuous networks.
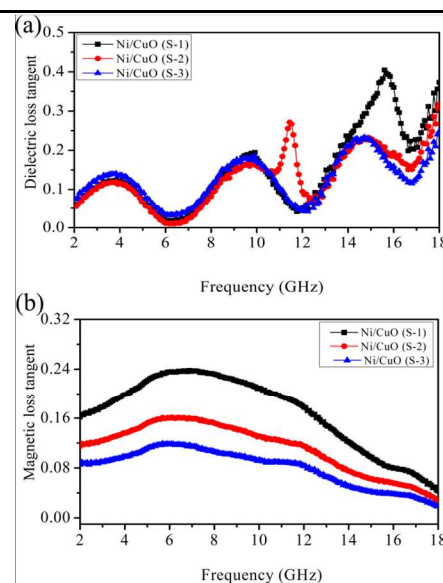

Figure 10. (a) The dielectric loss factor and (b) magnetic loss factor of Ni/CuO–paraffin wax samples versus frequency.

According to transmission line theory, effective absorbers are dominated by two key factors. One is the impedance match, which requires the complex permittivity and permeability to be equal, and the other is the EM attenuation in the interior absorber. The EM attenuation was determined by the attenuation constant α, which can be described as:[65, 66]

$$\alpha = \frac{\sqrt{2}\pi f}{c} \times \sqrt{\left(\mu''\varepsilon'' - \mu'\varepsilon'\right) + \sqrt{\left(\mu''\varepsilon'' - \mu'\varepsilon'\right)^2 + \left(\mu'\varepsilon'' + \mu''\varepsilon'\right)^2}} \quad (3)$$

where f is the frequency of the EM-wave and C is the velocity of light. Fig.11 shows the frequency dependence of the attenuation constant. The S-1 possesses biggest α in all frequency ranges, indicating the excellent attenuation or EM wave absorption. In the present case, based on the above equation, the higher imaginary parts of the permittivity and permeability seem to be useful for improving the attenuation constant. It is noted that high values of ε″ and μ″ would result in high α. The highest ε″ and μ″ values seem important for obtaining highest α. The enhancement of the EMA performance for the S-1 sample comes from the increase in dielectric loss and magnetic loss. Otherwise, the thin dielectric CuO coating introduces the metal/dielectric interfaces, at which the interface polarization also increases the dielectric attenuation.
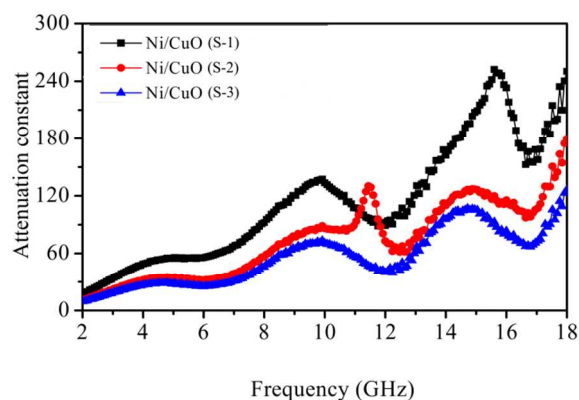

Figure 11. Attenuation constant of Ni/CuO–paraffin composites versus frequency.

It is well known that anti-oxidant capacity is an important criterion for material application. The oxidation behaviors of the pure Ni and Ni-CuO (S-1) are shown in **Fig.12**. The pure Ni begins to oxidize at around 263 ºC and. The pure Ni microspheres show a significant weight increase in the final stage owing to the oxidation in air at elevated temperatures. After coating with rice-like CuO shell, the Ni microspheres are protected, and the oxidation temperature is increased to about 372 ºC. It indicates that the core-shell Ni/CuO (S-1) presents better oxidization stability than that of Ni microsphere.
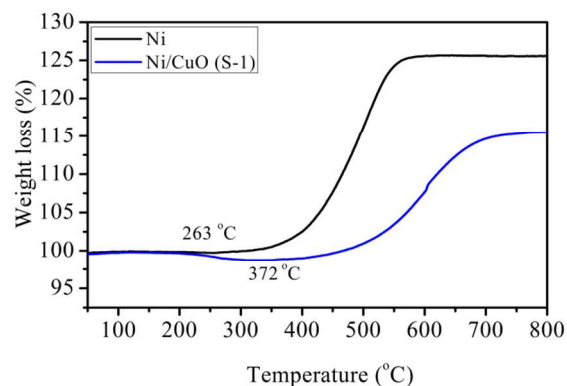

Figure 12. TG spectra of the Ni and Ni-R composite microspheres.

4. Conclusion

In summary, the hierarchical Ni/CuO heterostructures have been successfully synthesized by a two-step process. The as-prepared Ni/CuO products display a rice-like coating composites. Moreover, by tuning the molar ratio of the $CuCl_2 \cdot 2H_2O$ to the Ni microspheres, different shapes and coverage densities of CuO coating were obtained. The effects of CuO amounts on the Ni microspheres for microwave absorption properties have been investigated. The oxidation resistance of rice-like CuO-coated Ni composite is better than that of the pure Ni microsphere. The thin CuO-coated Ni composites (S-1) exhibit excellent electromagnetic properties. An optimal reflection loss is –62.2 dB at 13.8 GHz with the only thickness of 1.7 mm. The excellent microwave absorption properties are attributed to highest attenuation constant, interface polarization of core-shell structure and synergetic effect between the dielectric loss and magnetic loss. Our results demonstrate that the rice-like CuO-coated Ni core/shell composites with thin thickness and strong absorption are attractive candidates for the new types of EM wave absorptive materials.

Notes and references

[a] *School of Materials Science and Engineering, Zhengzhou University, Zhengzhou 450001, P.R.China*

[b] *Laboratory of Aeronautical Composites, Zhengzhou Institute of Aeronautical Industry Management, Zhengzhou 450046, China*

* Corresponding Author.

Dr. Gang Shao

E-mail address: gang_shao@zzu.edu.cn

Prof. Rui Zhang

Tel: +86-371-60632007

5 *Fax: +86-371-60632600*

E-mail address: zhangray@zzia.edu.cn

1.	J. Jiang, D. Li, D. Geng, J. An, J. He, W. Liu and Z. Zhang, *Nanoscale*, 2014, **6**, 3967-3971.

2.	H. Hekmatara, M. Seifi, K. Forooraghi and S. Mirzaee,
10	*Phys. Chem . Chem . Phys.,* 2014, **16**, 24069-24075.

3.	C. Hu, Z. Mou, G. Lu, N. Chen, Z. Dong, M. Hu and L. Qu, *Phys. Chem . Chem . Phys.*, 2013, **15**, 13038-13043.

4.	Y. Li, J. Zhang, Z. Liu, M. Liu, H. Lin and R. Che, *J.*
15	*Mater. Chem. C*, 2014, **2**, 5216-5222.

5.	T. K. Gupta, B. P. Singh, S. R. Dhakate, V. N. Singh and R. B. Mathur, *J. Mater. Chem. A*, 2013, **1**, 9138-9149.

6 .	 H. Yang, M. Cao, Y. Li, H. Shi, Z. Hou, X. Fang, H.
20	Jin, W. Wang and J. Yuan, *Adv. Opt. Mater.*, 2014, **2**, 214-219.

7.	G. Zou, M. Cao, H. Lin, H. Jin, Y. Kang and Y. Chen, *Powder Technol.*, 2006, **168**, 84-88.

8.	J. Yuan, H.-J. Yang, Z.-L. Hou, W.-L. Song, H. Xu, Y.-
25	Q. Kang, H.-B. Jin, X.-Y. Fang and M.-S. Cao, *Powder Technol.*, 2013, **237**, 309-313.

9.	X. Sun, J. He, G. Li, J. Tang, T. Wang, Y. Guo and H. Xue, *J. Mater. Chem. C*, 2013, **1**, 765-777.

10.	K. Singh, A. Ohlan, V. H. Pham, B. R, S. Varshney, J.
30	Jang, S. H. Hur, W. M. Choi, M. Kumar, S. K. Dhawan, B.-S. Kong and J. S. Chung, *Nanoscale*, 2013, **5**, 2411-2420.

11.	G. Li, L. Wang, W. Li, R. Ding and Y. Xu, *Phys. Chem . Chem . Phys.,*, 2014, **16**, 12385-12392.

35 12.	C. He, S. Qiu, X. Wang, J. Liu, L. Luan, W. Liu, M. Itoh and K.-i. Machida, *J. Mater. Chem.*, 2012, **22**, 22160-22166.

13.	D. Sun, Q. Zou, Y. Wang, Y. Wang, W. Jiang and F. Li, *Nanoscale*, 2014, **6**, 6557-6562.

40 14.	H. Guo, Y. Zhan, Z. Chen, F. Meng, J. Wei and X. Liu, *J. Mater. Chem. A*, 2013, **1**, 2286-2296.

15.	A. Ohlan, K. Singh, A. Chandra and S. K. Dhawan, *ACS Appl. Mater. Interfaces*, 2010, **2**, 927-933.

16.	J. Cao, W. Fu, H. Yang, Q. Yu, Y. Zhang, S. Liu, P.
45	Sun, X. Zhou, Y. Leng, S. Wang, B. Liu and G. Zou, *J. Phys. Chem. B*, 2009, **113**, 4642-4647.

17.	L. Du, Y. Du, Y. Li, J. Wang, C. Wang, X. Wang, P. Xu and X. Han, *J. Phys. Chem. C*, 2010, **114**, 19600-19606.

50 18.	X. F. Zhang, H. Huang and X. L. Dong, *J. Phys. Chem. C*, 2013, **117**, 8563-8569.

19.	J. Zhu, S. Wei, N. Haldolaarachchige, D. P. Young and Z. Guo, *J. Phys. Chem. C*, 2011, **115**, 15304-15310.

20.	W. Zhou, X. Hu, X. Bai, S. Zhou, C. Sun, J. Yan and P.
55	Chen, *ACS Appl. Mater. Interfaces*, 2011, **3**, 3839-3845.

21.	C. Cui, Y. Du, T. Li, X. Zheng, X. Wang, X. Han and P. Xu, *J. Phys. Chem. B*, 2012, **116**, 9523-9531.

22.	Y.-J. Chen, G. Xiao, T.-S. Wang, Q.-Y. Ouyang, L.-H.
60	Qi, Y. Ma, P. Gao, C.-L. Zhu, M.-S. Cao and H.-B. Jin, *J. Phys. Chem. C*, 2011, **115**, 13603-13608.

23.	Y.-J. Chen, F. Zhang, G.-g. Zhao, X.-y. Fang, H.-B. Jin, P. Gao, C.-L. Zhu, M.-S. Cao and G. Xiao, *J. Phys. Chem. C*, 2010, **114**, 9239-9244.

65 24.	Y.-J. Chen, P. Gao, R.-X. Wang, C.-L. Zhu, L.-J. Wang, M.-S. Cao and H.-B. Jin, *J. Phys. Chem. C*, 2009, **113**, 10061-10064.

25.	G. Tong, Q. Hu, W. Wu, W. Li, H. Qian and Y. Liang, *J. Mater. Chem.*, 2012, **22**, 17494-17504.

70 26.	C. Gong, J. Zhang, X. Zhang, L. Yu, P. Zhang, Z. Wu and Z. Zhang, *J. Phys. Chem. C*, 2010, **114**, 10101-10107.

27.	B. Zhao, B. Fan, G. Shao, B. Wang, X. Pian, W. Li and R. Zhang, *Appl. Surf. Sci.*, 2014, **307**, 293-300.

28. T. Liu, P. Zhou, J. Xie and L. Deng, *J. Appl. Phys.*, 2012, **111**, 093905.

29. C. Wang, X. Han, P. Xu, J. Wang, Y. Du, X. Wang, W. Qin and T. Zhang, *J. Phys. Chem. C*, 2010, **114**, 3196-3203.

30. X. Zhang, X. Dong, H. Huang, Y. Liu, W. Wang, X. Zhu, B. Lv, J. Lei and C. Lee, *Appl. Phys. Lett.*, 2006, **89**, 053115.

31. X. P. Gao, J. L. Bao, G. L. Pan, H. Y. Zhu, P. X. Huang, F. Wu and D. Y. Song, *J. Phys. Chem. B*, 2004, **108**, 5547-5551.

32. B. Pecquenard, F. Le Cras, D. Poinot, O. Sicardy and J.-P. Manaud, *ACS Appl. Mater. Interfaces*, 2014, **6**, 3413-3420.

33. F. Zhang, A. Zhu, Y. Luo, Y. Tian, J. Yang and Y. Qin, *J. Phys. Chem. C*, 2010, **114**, 19214-19219.

34. G. Zhu, H. Xu, Y. Xiao, Y. Liu, A. Yuan and X. Shen, *ACS Appl. Mater. Interfaces*, 2012, **4**, 744-751.

35. M. Zhou, Y. a. Gao, B. Wang, Z. Rozynek and J. O. Fossum, *Eur. J. Inorg. Chem.*, 2010, **2010**, 729-734.

36. A. Kargar, Y. Jing, S. J. Kim, C. T. Riley, X. Pan and D. Wang, *ACS Nano*, 2013, **7**, 11112-11120.

37. J. Zeng, J. Xu, P. Tao and W. Hua, *J. Alloys Compd.*, 2009, **487**, 304-308.

38. J. Zeng, H. Fan, Y. Wang, S. Zhang, J. Xu and X. Cheng, *Thin Solid Films*, 2012, **520**, 5053-5059.

39. J. Zeng, P. Tao, S. Wang and J. Xu, *Appl. Surf. Sci.*, 2009, **255**, 4916-4920.

40. X. Liu, C. Feng, S. W. Or, Y. Sun, C. Jin, W. Li and Y. Lv, *RSC Adv.*, 2013, **3**, 14590-14594.

41. B. Zhao, G. Shao, B. Fan, W. Li, X. Pian and R. Zhang, *Mater. Lett.*, 2014, **121**, 118-121.

42. C. Kong, L. Tang, X. Zhang, S. Sun, S. Yang, X. Song and Z. Yang, *J. Mater. Chem. A*, 2014, **2**, 7306-7312.

43. X.-J. Zhang, G.-S. Wang, W.-Q. Cao, Y.-Z. Wei, J.-F. Liang, L. Guo and M.-S. Cao, *ACS Appl. Mater. Interfaces*, 2014, **6**, 7471-7478.

44. Y. Du, T. Liu, B. Yu, H. Gao, P. Xu, J. Wang, X. Wang and X. Han, *Mater. Chem. Phys.*, 2012, **135**, 884-891.

45. S. He, G.-S. Wang, C. Lu, J. Liu, B. Wen, H. Liu, L. Guo and M.-S. Cao, *J. Mater. Chem. A*, 2013, **1**, 4685-4692.

46. X.-L. Shi, M.-S. Cao, J. Yuan, Q.-L. Zhao, Y.-Q. Kang, X.-Y. Fang and Y.-J. Chen, *Appl. Phys. Lett.*, 2008, **93**, 183118.

47. X. Liu, G. Zhou, S. W. Or and Y. Sun, *RSC Adv.*, 2014, **4**, 51389-51394.

48. T. Chen, F. Deng, J. Zhu, C. Chen, G. Sun, S. Ma and X. Yang, *J. Mater. Chem.*, 2012, **22**, 15190-15197.

49. Y. Naito and K. Suetake, *IEEE Trans. Microwave Theory Tech.*, 1971, **19**, 65-72.

50. J. J. Pesque, D. P. Bouche and R. Mittra, *IEEE Trans. Microwave Theory Tech.*, 1992, **40**, 1789-1796.

51. S. S. Kim, S. B. Jo, K. I. Gueon, K. K. Choi, J. M. Kim and K. S. Churn, *IEEE Trans. Magn.,* 1991, **27**, 5462-5464.

52. M. Cao, R. Qin, C. Qiu and J. Zhu, *Mater. Des.*, 2003, **24**, 391-396.

53. M.-S. Cao, J. Yang, W.-L. Song, D.-Q. Zhang, B. Wen, H.-B. Jin, Z.-L. Hou and J. Yuan, *ACS Appl. Mater. Interfaces*, 2012, **4**, 6949-6956.

54. Y. Chen, X. Liu, X. Mao, Q. Zhuang, Z. Xie and Z. Han, *Nanoscale*, 2014, **6**, 6440-6447.

55. X. Chen, F. Meng, Z. Zhou, X. Tian, L. Shan, S. Zhu, X. Xu, M. Jiang, L. Wang, D. Hui, Y. Wang, J. Lu and J. Gou, *Nanoscale*, 2014, **6**, 8140-8148.

56. Z. Wang, L. Wu, J. Zhou, Z. Jiang and B. Shen, *Nanoscale*, 2014 ,**6**, 12298-12302

57. R. Li, T. Wang, G. Tan, W. Zuo, J. Wei, L. Qiao and F. Li, *J. Alloys Compd.*, 2014, **586**, 239-243.

58. C. Wang, X. Han, X. Zhang, S. Hu, T. Zhang, J. Wang, Y. Du, X. Wang and P. Xu, *J. Phys. Chem. C*, 2010, **114**, 14826-14830.

59.   N. Ortega, A. Kumar, R. Katiyar and C. Rinaldi, *J. Mater. Sci.*, 2009, **44**, 5127-5142.

60.   S. Wen, Y. Liu, X. Zhao, J. Cheng and H. Li, *J. Magn. Magn. Mater.*, 2014, **354**, 7-11.

61.   Q. Liu, D. Zhang and T. Fan, *Appl. Phys. Lett.*, 2008, **93**, 013110.

62.   X. G. Liu, D. Y. Geng, H. Meng, P. J. Shang and Z. D. Zhang, *Appl. Phys. Lett.*, 2008, **92**, 173117.

63.   R. F. Zhuo, L. Qiao, H. T. Feng, J. T. Chen, D. Yan, Z. G. Wu and P. X. Yan, *J. Appl. Phys.*, 2008, **104**, 094101.

64.   R. F. Zhuo, H. T. Feng, J. T. Chen, D. Yan, J. J. Feng, H. J. Li, B. S. Geng, S. Cheng, X. Y. Xu and P. X. Yan, *J. Phys. Chem. C*, 2008, **112**, 11767-11775.

65.   S. Yan, L. Zhen, C. Xu, J. Jiang and W. Shao, *J. Phys. D: Appl. Phys.*, 2010, **43**, 245003.

66.   B. Lu, H. Huang, X. L. Dong, X. F. Zhang, J. P. Lei, J. P. Sun and C. Dong, *J. Appl. Phys.*, 2008, **104**, 114313.